Heterogeneous exhumation in the Inner Moray Firth, UK North Sea: constraints from new AFTA® and seismic data

J.D. Argent[1], S.A. Stewart[2], P.F. Green[3] and J.R. Underhill[4]

[1]Amerada Hess Corporation, 6688 North Central Expressway, Suite 1400, Dallas, Texas 75206-3925, USA

[2]BP, Burnside Road, Farburn Industrial Estate, Dyce, Aberdeen, AB21 7PB, UK

[3]Geotrack International Pty Ltd, 37 Melville Road, West Brunswick, Victoria 3055, Australia

[4]Department of Geology & Geophysics, The University of Edinburgh, Grant Institute, King's Buildings, West Mains Rd, Edinburgh, EH9 3JW, UK

Abstract

Integration of regional seismic interpretation, sonic velocity, vitrinite reflectance and apatite fission track analysis (AFTA®) studies has demonstrated that the western region of the Moray Firth rift arm (UK North Sea) experienced pronounced exhumation during the Cenozoic. Although this basin is usually considered to have experienced regionally uniform exhumation, interpretation of new seismic data has revealed the presence of a major system of post-Jurassic normal faults, with throws commonly in the range of 10-300m, and locally exceeding 1km. The new, high quality seismic data are used in combination with apatite fission track analysis and vitrinite reflectance data to investigate the role of extensional faulting during exhumation of this basin. Results not only confirm the offsets across major faults, they show that greater exhumation and erosion occurred on their footwalls compared to hangingwalls. We conclude that the localised, differential exhumation is the result of superposition of local or short wavelength extensional tectonics upon regional, long wavelength exhumation. These results suggest that differential exhumation might be characteristic of unroofed rift basins where normal faults subcrop the exhumation-related unconformity and that in such cases, thermal histories from footwall locations may yield inaccurate predictions of the burial history of hangingwall depocentres and thus, misrepresents maturity estimates.

Keywords: North Sea, Moray Firth, exhumation, structural inversion, AFTA

Accepted for publication in the Journal of the geological Society

The Moray Firth rift basin is located on the western arm of the UK North Sea Upper Jurassic trilete rift-system. Stratigraphic datums in the western extremity of the Moray Firth basin, the Inner Moray Firth, are approximately 500-1500m shallower than they are in the Viking and Central Graben areas to the east. The shallower depth of Jurassic sediments, and the major seabed unconformity in the Inner Moray Firth is generally regarded as the result of early Tertiary exhumation[1] (Underhill 1991; Hillis *et al.* 1994).

The deep structure of the Inner Moray Firth basin is dominated by numerous extensional tilted fault blocks that were active during the Late Jurassic syn-rift episode (Underhill 1991a). The basin's overall configuration is defined by three major fault systems; the Wick Fault on the northern margin, the Banff Fault to the south and the Helmsdale Fault to the west (**Figure 1a**). Newly acquired seismic data has allowed detailed mapping of the entire basin structure bounded by these fault systems (**Figure 1a**). The purpose of this paper is to integrate this new structural interpretation with direct measurements of exhumation from wells in the basin, using new apatite fission track analysis (AFTA®) and vitrinite reflectance data obtained from deep exploration wells in the basin interior, in order to more fully understand the kinematics of post-Jurassic basin evolution. Based on these results, specifically from two exploration wells, we present here a new model of partitioned net exhumation for this basin.

Database

The seismic database consists of over 2500km of regional 2D seismic lines. Line spacing is generally in the order of 1-2km. Well data consists of 54 penetrations, almost all drilled to depths in excess of 2,500m (**Figure 1a**). New AFTA data have been made available to this study from a number of these wells and onshore locations, but we examine in detail two offshore exploration wells, 12/23-1 and 12/24-2 (**Figure 1a**). These two wells are located with 5km separation on either side of the Smith Bank Fault and are conveniently placed to compare the exhumation on either side of this major fault (**Figure 1a**). These new offshore AFTA data were integrated with new vitrinite reflectance measurements to give estimates of the magnitude and timing of exhumation.

[1] In this paper we use the term 'exhumation' to refer to height above maximum burial depth relative to the datum of present day mean sea level.

Data Analysis: Evidence for presence, timing and magnitude of basin exhumation

Regional Seismic Mapping

Tilt of the whole of the western area of the North Sea is apparent from regional studies of seismic and well data (Underhill, 1991a; Underhill & Partington 1993; Japsen 1997; 1999). This tilt is responsible for the relative elevation of the Inner Moray Firth in comparison with the deeper North Sea sub-basins further east. Seabed subcrop mapping within the Inner Moray Firth confirms the easterly dip of the strata (Andrews et al. 1990; Figure 1a). The stratigraphic column penetrated to date by exploratory wells within the Moray Firth is illustrated in Figure 1b. The complete section spans the Devonian to Tertiary. However, in the Inner Moray Firth the uppermost section of the Upper Cretaceous Chalk Group and any subsequent Tertiary sequences are absent. East-west trending seismic lines that pass from the Inner to Outer Moray Firth show the Upper Cretaceous Chalk Group and earliest Palaeocene sediments are truncated at the seabed, implying that exhumation began after Chalk Group deposition in the Tertiary (see figure 4 in Argent et al. 2000). Argent et al. (2000) point out that the Chalk Group is the cause of many sub-Cretaceous seismic imaging problems in the North Sea, even with recent high fidelity data. Its absence from the Inner Moray Firth results in improved image quality enabling correlations across faulted Lower Cretaceous and Jurassic sections to be made with a high degree of confidence. As indicated in Figure 1, most of the wells in the basin were available to this study and were used to constrain the seismic interpretation. Present day Base Jurassic structure as mapped in this study is shown in Figure 2. The quality of data on which this mapping is based and the nature of the structures themselves is shown in Figure 3, which illustrates an Upper Jurassic syn-rift package growing into the major extensional sub-basinal faults in the middle of the basin (Underhill, 1991b). The largest faults in the Inner Moray Firth have up to 2km offset of the Base Jurassic reflector. However, these large sub-basin bounding faults also offset the Base Cretaceous (Figure 3) and the Base Tertiary, with throws in the range 10 - 300 metres. Therefore, although these structures are principally Mesozoic in age, they have a significant post-Jurassic history of reactivation that is essentially absent from the deeper North Sea sub-basins (e.g. Underhill 1998). Some minor movement may have occurred during the deposition of the earliest Lower Cretaceous, Hauterivian Stage (Figure 3). This movement is in the order of tens of metres of displacement on the Smith Bank Fault, indicated by the minor sequence thickening towards the fault in the earliest section of the Lower Cretaceous. Correlation of footwall to hangingwall reflectors suggests that subsequent Cretaceous deposition was not associated with any further extensional fault movement. The most significant component of extensional reactivation of these structures was post-Cretaceous, indicated by mapped offsets of the top and base Cretaceous across the main faults in the basin (Figure 1).

Vitrinite Reflectance (VR)

A plot of VR data against depth from Inner Moray Firth exploration wells (**Figure 4**) shows a wide variance of values, although individual wells exhibit consistent reflectance gradients. The vast majority of the VR data here has been determined in the organic-rich source unit of the Upper Jurassic Kimmeridge Clay Formation, often resulting in anomalously low VR estimates due to suppression effects. Unfortunately, it is not known if this combined dataset from a variety of released commercial studies consistently incorporates the variable absorption of sapropelic material within the marine clays of the Upper Jurassic shales, which may lower VR values. Large amounts of bitumen (Hutton *et al*. 1980) and oil-prone macerals (Price & Barker 1985) retard the normal increase of vitrinite reflectance with maturity in such source shale intervals.

Notwithstanding the scatter in the dataset as a whole, the VR recorded by the majority of the wells is found to be higher than that expected for its equivalent sample depth when compared to their counterparts in the Outer Moray Firth. A reasonable explanation for this disparity is relative exhumation of the samples from the Inner Moray Firth compared to those in the Outer Moray Firth resulting in higher apparent VR values for a given depth. In contrast, a sustained period of elevated heat flow in the region of the Inner Moray Firth would cause an offset that increases with depth. If heat flow in the region has remained close to present-day values, extrapolation of data from individual wells in **Figure 4** to surface values for unheated vitrinite (the vitrinite reflectance of wood is 0.2%) implies exhumation in the range 500-2000m.

Sonic Velocity Data

Hillis *et al*. (1994) showed that sonic velocity data for the Chalk and Kimmeridge Clay Formation shales in the Inner Moray Firth are consistent with their being over-compacted with respect to their present-day depth. This suggests that the section has been exhumed to some degree from their maximum burial depths (**Figure 5**). Hillis *et al*. (1994) showed that these results contrast with those obtained from the Outer Moray Firth, where formations show no sign of overcompaction. Since there is no significant change in shale composition between the Inner Moray Firth and Outer Moray Firth, such overcompaction can only be explained by exhumation of the sediments from deeper burial depths. This is in agreement with the other evidence for exhumation of the Inner Moray Firth basin discussed so far. Estimates of the amount of exhumation of individual Inner Moray Firth wells range from 580-1280m. Although there was a significant spatial variation in the degree of exhumation between wells (**Figure 5**), Hillis *et al.* (1994) did not attempt to relate this to the underlying basin structure.

Apatite Fission Track Analysis (AFTA)

Method

AFTA is based on measurement of naturally occurring radiation damage trails or "fission tracks" caused by the spontaneous fission of Uranium within detrital apatite grains, which are a common constituent of most sandstones. The technique exploits the self healing property of these tracks, which form at a constant rate through time, and then shorten ("anneal") at a temperature-dependent rate. By measuring a "fission track age" (based on the number of tracks in a polished apatite grain surface) and the distribution of track lengths**,** it is possible to estimate the maximum palaeotemperature attained by a rock sample and the time at which the sample began to cool towards the present-day temperature. AFTA procedures and examples are described in detail in several publications (e.g. Green *et al.* 1989a; 1989b; Bray *et al.* 1992).

The capacity of AFTA to provide an independent determination of the timing at which cooling began is particularly useful in the reconstruction of thermal and burial histories of sedimentary basins, especially if there are unconformities representing large time gaps (Duncan *et al.* 1998). In the case of the Inner Moray Firth, the Cretaceous and Tertiary sections that are present elsewhere in the North Sea are absent. Their absence is due either to exhumation and erosion of the section, or non-deposition. The evidence discussed so far (seismic, VR, sonic) has indicated that exhumation and erosion was responsible. AFTA provides a further, independent, means of testing this and has the potential to yield estimates of timing in addition to the magnitude of basin exhumation.

Combined AFTA and VR in the determination of exhumation magnitudes

The combined interpretation of the thermal history of both AFTA and VR data begins by assessing whether the fission track age and track length data in each sample (and/or the VR value) could have been produced if the down-hole sample had never been hotter than the present-day temperature at any time since its deposition. A burial history derived from progressively removing the overlying preserved sedimentary section is combined with the present-day geothermal gradient to construct a "Default Thermal History" for each sample. Using this history, default AFTA and VR parameters can be modelled for each sample. If the observed data are consistent with the values predicted from this default history, then the sample is at or close to its maximum post-depositional temperature. If, however, the data show a greater degree of fission track annealing or VR maturity than expected on the basis of this default history, the sample must have been hotter in the past than it is at the present day depth of burial. In such cases, AFTA provides an estimate of the time at which cooling began, and both AFTA and VR constrain the magnitude of the maximum palaeotemperature reached by individual samples. For further details on the thermal history response of fission tracks in

apatite, the development of AFTA parameters, and the use of AFTA and VR to extract thermal history solutions in sedimentary basins, see Green *et al*. (2001a; 2001b) and Green *et al*. (in press).

Analysis of samples and determination of palaeotemperatures over a range of depths within a vertical well section allows determination of the palaeogeothermal gradient at the onset of cooling. From extrapolation of the palaeogeothermal gradient to an assumed palaeo-surface temperature allows an estimation of the amount of missing section to be determined (**Figure 6**). This provides a measure of the magnitude of exhumation. Combining results from AFTA and VR has two advantages. Firstly, since each technique is calibrated independently, results from the two methods provide independent verification of the results from the other. And secondly, the joint approach also affords the opportunity to obtain data from various lithologies through the well, to provide palaeotemperature assessment over as wide a depth interval as possible (allowing more precise constraints on palaeogeothermal gradients and removed section).

Results from two Inner Moray Firth wells

Wells 12/23-1 and 12/24-2 were selected due to their proximity to one another on adjacent margins of a major sub-basinal extensional fault (Smith Bank Fault). Well 12/23-1 is located in the footwall and 12/24-2 is located in the hangingwall section (**Figure 1**). AFTA data in six samples from these two wells are summarised in Table 1. AFTA parameters in each well (fission track ages and mean track lengths) are plotted as a function of depth and present temperature in **Figure 7**, where the fission track age data are contrasted with the variation of stratigraphic age through the section.

Qualitative examination of the AFTA parameters from these wells shows significant contrasts that suggest major differences in the thermal history of the sequences in these two wells. For instance, fission track ages in samples from well 12/23-1 in **Figure 7** show a more rapid decrease with depth/temperature compared to results from well 12/24-2, and at depths around 2600 metres the mean track length is shorter in well 12/23-1 compared to well 12/24-2.

This point is further emphasised in **Figure 8**, which shows the pattern of fission track age versus chlorine content in sample GC237-30 from well 12/23-1 and sample GC237-55 from well 12/24-2. Most common apatites are fluorine rich, however they may contain appreciable amounts of chlorine. The amount of chlorine in the apatite lattice exerts an important compositional control on the degree of fission track annealing. Apatites richer in fluorine are more easily annealed than those richer in chlorine. The result of this effect is that in a single sample, individual apatite grains may show a spread in the degree of annealing. This effect

becomes more pronounced at temperatures ranging from 90-120°C and can therefore be useful when dealing with samples exposed to temperatures in this higher range (Green *et al*. 1996).

For each sample, the measured ages are contrasted with the pattern of age versus Chlorine content predicted from the respective Default Thermal History for each sample. These results illustrate a key difference between the two samples, taken from present-day temperatures of 80°C and 90°C, respectively. Given that the Default Thermal Histories for both samples involve residence at or above these temperatures for at least 65 million years, representing the present day sea bed unconformity in each well, we might expect a slightly greater degree of annealing (age and length reduction) in sample GC237-55 (from 90°C in well 12/24-2) compared to sample GC237-30 (from 80°C in well 12/23-1). In fact, since the seabed unconformity in well 12/23-1 represents a longer interval than that in well 12/24-2, the predicted degrees of annealing are very close in the two samples despite the lower present-day temperature of GC237-30, as shown by the predicted lengths in Table 2. But the measured data show a very different pattern. In sample GC237-30, all measured ages are much less than the values predicted from the Default Thermal History, showing that this sample has been hotter in the past. In contrast, measured ages in sample GC237-55 are either close to, or greater than the values predicted from the Default Thermal History, suggesting that this sample has not been appreciably hotter than its present-day temperature at any time since deposition.

Quantitative thermal history interpretation of AFTA and VR data from these wells (following principles outlined in Green *et al*. 2001a; 2001b & in press) is summarised in Table 2. This confirms the qualitative differences discussed above, and reveals further details of the thermal history of the sequences intersected in each well, as discussed in the following sections.

12/23-1

Fission track age and mean track length data were analysed for four samples at various depths within this well (Table 1). The AFTA results, taken as a whole, show that each sample has cooled from a higher temperature in the past. This evidence comes from the track length data in samples GC237-27, -28 and -29, which show a greater degree of reduction in track length than can be explained using the Default Thermal History (Table 2), and from fission track age data in sample GC237-30, which show a greater degree of age reduction than can be explained by the Default Thermal History (Table 2 and **Figure 7**).

Estimates of the magnitude of maximum palaeotemperatures and the time at which cooling from those palaeotemperatures began, derived from the AFTA data in each sample, are summarised in Table 2. Maximum palaeotemperatures increase downhole, from 65-85°C in sample GC237-27 to greater than 100°C in sample GC237-30. Assuming that the data from

all the samples represent a common thermal event, comparison of the timing constraints from all four samples would be consistent with a single episode of cooling beginning sometime between 100 and 40 Ma, consistent with an early Tertiary event. AFTA data from a larger number of wells in the Inner Moray Firth, also analysed as part of this study (not fully reported here), allows this timing to be refined further to the interval 60 to 55 Ma, showing that the sampled units began to cool from maximum post-depositional paleotemperatures in the Early Tertiary (**Figure 9**). All these samples illustrated in **figure 9** broadly suggest an early Tertiary age for the onset of cooling within 95% confidence limits. However, by combining the data for all the samples a refined timing of 55-60 Ma for the onset of cooling is found via overlap of the sample cooling ranges. A single sample, from well 12/29-1, is excluded from this interpretation. The onset of cooling for this sample is later, sometime between 0-20Ma and is inconsistent with that derived from all other wells and outcrop locations. Whether these data are genuine, or are some kind of analytical artefact is not known at present. On this basis, we feel that the palaeothermal effects recognised in 12/29-1 are probably best interpreted in terms of the same Early Tertiary episode recognised in the other samples. However, the possibility of a real difference in timing, with a later onset of cooling for the Banff High on which 12/29-1 is located cannot be ruled out.

VR from down-hole samples in well 12/23-1 are shown in **Figure 4**. As summarised in Table 2, two VR values from the Barremian section and one from the Lower Permian are higher than the values predicted by the respective Default Thermal History, suggesting that these units have been hotter in the past compared to their present day temperatures. In contrast, VR values from the Upper Jurassic units in this well give anomalously low offset from the Default Thermal History compared with other samples from this well. This is probably due to the sapropelic rich character of the Upper Jurassic Kimmeridge Clay Formation, which is not considered to provide a reliable measurement of the true thermal maturity of this well. Maximum palaeotemperatures derived from the VR data in this well using the kinetic model of Burnham and Sweeney (1989) increase downhole from less than 50°C in the Early Cretaceous section to 92°C in the Permian section (Table 2).

The combined palaeotemperature constraints from the VR and AFTA in well 12/23-1 are shown plotted against depth in **Figure 10a**. Those derived from the AFTA are consistent with those from the VR data at similar depths with the exception of the suppressed VR values obtained from the Upper Jurassic, which are much lower than the palaeotemperatures suggested by AFTA. Apart from the Upper Jurassic VR, both the AFTA and VR data therefore represent the same episode of heating.

Figure 10a shows that the AFTA and VR data both define a linear depth profile, sub-parallel to the present day temperature profile but offset to a higher temperature by between 30° and

50°C. This profile therefore suggests that the observed palaeotemperatures could be explained largely in terms of extra heating due to additional depth of burial, with subsequent cooling due to exhumation and erosion. The timing of this cooling event indicated by AFTA (100 to 40 Ma) coincides with a pronounced unconformity at a depth of 135m in this well, across which the Barremian to Pleistocene section is absent. Therefore deeper burial, and subsequent exhumation during this interval provides a viable explanation of the observed early Tertiary palaeotemperatures in this well.

12/24-2

Results from the two AFTA samples taken from well 12/24-2 match the Default Thermal History predictions (**Figure 7**, Table 2). The maximum limit of 125°C set by the data from sample GC237-56 is only 4°C above the present day temperature of 121°C at this depth, suggesting that only a very limited amount of additional heating may have affected this sample.

Palaeotemperature constraints from VR in this well are plotted against depth in **Figure 10b**. Values derived from these VR data are lower than the present-day temperature profile. Maximum palaeotemperatures derived from the VR data vary between 69°C and 95°C suggesting that these VR data are anomalously low and are interpreted as having been sapropelically suppressed since these samples were taken within the Upper Jurassic Kimmeridge Clay Formation. Alternatively, the present-day geothermal gradient may be lower than that used in calculating the profile. At present there is no way of discriminating between these two possibilities, however the present-day geothermal gradient of 32.4°C/km is comparable to that of 12/23-1 with a present-day gradient of 29.7°C/km taken from temperature measurements made whilst wireline logging of these wells was completed.

The combined results from AFTA and VR from both these down-hole samples show no clear evidence of transient palaeogeothermal anomalies in the section, and the most likely explanation of the data is that all the units throughout the well are currently at or close to their maximum temperatures since deposition. We conclude that the VR results from this well consist of anomalously suppressed values, since the present-day thermal gradient of 32.4C/km (from corrected borehole temperatures) is not unusually high and is consistent with geothermal gradients measured in other Inner Moray Firth wells.

Calculation of exhumation magnitude from wells 12/23-1 and 12/24-2

Estimates of the maximum palaeotemperatures from samples taken over a vertical depth range, such as from an exploration well, provides the capability of determining the palaeogeothermal gradient immediately prior to the onset of cooling. Having constrained the palaeogeothermal gradient and assuming a value for the surface temperature at the time, the

amount of section subsequently removed by exhumation and erosion can be calculated as illustrated in **Figure 6**. The total amount of section removed is obtained by dividing the difference between the palaeo-surface temperature (Ts) and the intercept of the temperature profile at the appropriate (Ti) by the estimated palaeogeothermal gradient. This method relies on the assumption that the temperature profile was linear both throughout the section analysed and through the overlying section that has been removed. Consistency between estimates of eroded section derived in this way and other estimates such as seismic sections suggest that this assumption should be valid (Green *et al*. 1995).

The calculated Early Tertiary paleotemperature profile in well 12/23-1 is linear and sub-parallel to the present-day temperature profile (with a gradient of approximately 30ºC/km in each case) supporting the evidence discussed above that heating was mainly due to additional depth of burial (with subsequent cooling due to exhumation) rather than elevated, transient heat flow. An estimate of the thickness of section eroded from the sea bed unconformity can be made by making a linear extrapolation of the present-day and palaeogeothermal gradients to a surface temperature of 6°C. This method yields 1.05-1.25km of missing section from well 12/23-1.

In contrast, results from well 12/24-2 do not require any appreciable amount of eroded section. This indicates a significant variation in the amount of exhumation between these two wells, in spite of their limited spatial separation (5km). However, the wells lie either side of the Smith Bank Fault, a major normal fault that is seen to have a history of post-Jurassic extensional movement on seismic data. A possible alternative interpretation is that the palaeogeothermal gradient in well 12/24-2 could have been underestimated, such that the section was hotter in the past, therefore allowing some degree of Tertiary exhumation and erosion. However, the amounts of removed section must be quite small as the Chalk Group is still present in the shallow section of the well and some degree of structural control would still be required to explain the differences in thickness of the preserved section between the two wells.

Integration of AFTA and VR results with seismic imaging of Smith Bank Fault

A seismic line tying wells 12/23-1 and 12/24-2 illustrates the post-Jurassic history of extensional movement on the Smith Bank Fault (**Figure 11**). Mapping of the whole dataset shows that the majority of this displacement is post-Cretaceous (**Figure 1**). The depths to Base Jurassic and Base Cretaceous in the wells, tied to the seismic image indicate that there has been 2,350m of post Triassic displacement on the Smith Bank Fault, of which 750m is post-Jurassic. Uncertainty in these estimates arises principally from seismic time to depth

conversion away from the well control and we estimate that the error in these measurements is less than 30m. Differential burial between these two wells was estimated at 670m in the sonic velocity study of Hillis *et al*. (1994) at the level of the Base Cretaceous. This matches the integrated AFTA and VR data results obtained in this study, which additionally suggest that cooling commenced 55-60Ma. Although the thermal history reconstruction may have marginally overestimated the amount of exhumation, this may be indicative of uncertainty in the palaeogeothermal gradient estimation. In addition, results from the 12/24-2 well would allow a small amount of removed section in that well, with cooling of 5 to 10°C equivalent to approximately 150-300 metres of missing section which could not be resolved within the palaeotemperature data (since post-Chalk sediments are missing in well 12/24-2, some degree of erosion must have occurred at this site). So these results are all consistent with the seismically observed post-Jurassic offset of 750±30m. The majority of these large sub-basinal bounding faults in the Inner Moray Firth exhibit some degree of post-Jurassic fault reactivation (**Figure 1**), and similar to the Smith Bank Fault, these faults are truncated at the seabed.

Kinematics of basin exhumation

Here we synthesise the observations and interpretations presented so far into a tectonic model representing basin exhumation. Rather than choose a specific model straight away, we first define three end member kinematic options, each model characterised by various combinations of regional exhumation (on a wavelength of 100's km) and fault tectonics (**Figure 12**). The effects of the endmember models are depicted in relation to an initial rift basin template (**Figure 12a**) that is intended to represent the geometry of the Inner Moray Firth at the end of the Cretaceous.

In the following discussion we choose a preferred model. The first possibility shown in **Figure 12b** has little or no contribution from intra-basinal faulting during regional uplift and can be termed epeirogenic exhumation (Hallam 1963; McKenzie 1984). Epeirogenic exhumation would lead to smooth, progressive variations in exhumation of flat, regional stratigraphic markers (**Figure 12b**), as noted elsewhere on the Atlantic margins (e.g. Pazzaglia & Gardner 1994; Rohrman & van der Beek 1996). The spatial variations in amount of exhumation suggested by previously published studies (Hillis *et al*.1994) and confirmed by the investigation of the Smith Bank Fault presented here, suggest that local, differential exhumation has been important and we rule out epeirogenic exhumation as shown in **Figure 12b** as the single mechanism responsible for basin inversion of the Inner Moray Firth.

At the other extreme, reverse faulting could cause the pattern of exhumation and basin inversion – the differential exhumation of 12/23-1 relative to 12/24-2 could be accounted for if well 12/23-1 lay in an overthrust block. This defines a second kinematic possibility – basin wide inversion controlled by reverse reactivation of extensional faults, with or without a background signature of epeirogenic exhumation, giving a heterogeneous picture of basin inversion (**Figure 12c**), perhaps better accounting for the rapid local variations in degree of exhumation suggested by various Inner Moray Firth studies. This type of heterogeneous inversion occurred during the Cretaceous and Tertiary on the south margin of the southern North Sea (Badley *et al.* 1989). However, the seismic data (**Figure 11**) clearly shows that the Smith Bank fault is an extensional fault dipping to the southeast and not a reverse fault dipping to the northwest required by the 12/23-1 data. We rule out this option due to the incompatibility between the kinematics of this model and the data from 12/23-1.

A third kinematic model combines a background of regional exhumation accompanied by extensional faulting (**Figure 12d**). The displacement across extensional faults is usually partitioned approximately 17:3 between hangingwall subsidence and footwall exhumation relative to local datums (Jackson *et al*. 1988; Gibson *et al*. 1989). However, if the entire area that is being extensionally faulted is simultaneously regionally exhumed, the net movement of hangingwall and footwall relative to regional datums will be a function of both processes. Both sides of the extensional fault may become exhumed relative to regional datums, in spite of extension across the fault (**Figure 12d**). Downthrow of the hangingwall is essentially buffered by the regional exhumation. We propose that this third kinematic model accounts for the spatial variation in exhumation observed in the various lines of evidence from Inner Moray Firth discussed in this paper. This model accounts for the curious phenomenon of wells in hangingwall lows exhibiting conventional, non-exhumed thermal histories while adjacent wells on footwalls highs can show significant amounts of exhumation. The model reconciles documented regional uplift of the west margin North Sea basin (Rohrman & van der Beek 1996; Japsen 1997) and post-Jurassic basement-linked extensional fault reactivation, which is restricted to the Inner Moray Firth (Underhill, 1991a; Stewart 1996; Underhill 1998). Note that in adopting this model we do not suggest any genetic link between the regional exhumation and the extensional faulting in the Inner Moray Firth. The Cenozoic extensional faulting in the Inner Moray Firth basin demonstrated here may also have occurred onshore and contributed displacement to fault contacts in the deeply eroded basement of the Scottish Highlands (c.f. Roberts & Holdsworth 1999).

This model of heterogeneous finite exhumation has implications for petroleum systems modelling. Had well data from the hangingwalls in this basin been scarce or absent, the magnitude of hangingwall burial might have been overestimated, since the missing section observed in the wells drilled into structural traps on the footwall highs could have been

projected into pseudo-wells in the hangingwall lows. This would lead to an erroneous estimate of kerogen maturity in the kitchen areas within the basin.

The net result of the tectonic model described in this paper is partitioning of exhumation across extensional faults. It is not presently known how extensive this phenomenon is along the western margin of the North Sea, or the eastern margin of the Atlantic. However, it is possible that this effect may be found wherever Mesozoic faults are exhumed to the seabed or surface and exhumation data measured in adjacent fault blocks should be projected across these faults after some circumspection.

Conclusions

A synthesis of seismic, apatite fission track analysis and vitrinite reflectance data from the Inner Moray Firth Basin shows significant local variations in Cenozoic exhumation across extensional faults. We account for these observations with a kinematic model of differential basin exhumation consisting of superposition of regional, epeirogenic exhumation, and local, short wavelength extensional faulting. Whilst the hangingwall of the extensional faults is of same order as the degree of 'regional' exhumation, the true nature and extent of 'basin inversion' appears only to have been recorded in their footwalls.

Acknowledgements

The views expressed here are solely those of the authors and do not necessarily represent those of the Amerada Hess Corp, BP Plc or Geotrack International Pty Ltd or any associated partner companies. AFTA® is a registered trademark owned and maintained by Geotrack International Pty Ltd. We are grateful to Peter Broad of Fugro Geoteam A/S for permission to show examples of recent seismic data from the region, and Colin Tannock of Talisman Energy UK Ltd for permission to publish the AFTA data. This manuscript benefited from thorough review and helpful advice from Joe Cartwright (Cardiff University) and Jonathan Turner (Birmingham University).

References

Andrews, I.J., Long, D., Richards, P.C., Thomson, A.R., Brown, S., Chesher, J.A. & McCormac, M. 1990. *United Kingdom offshore regional report: the geology of the Moray Firth*. HMSO for the Geological Society, London.

Argent, J.D., Stewart S.A. & Underhill, J.R. 2000. Controls on the Lower Cretaceous Punt Sandstone Member, a massive deep-water clastic deposystem, Inner Moray Firth, UK North Sea. *Petroleum Geoscience*, **6**, 275-285.

Badley, M.E., Price, J.D. & Backshall, L.C. 1989. Inversion, reactivated faults and related structures: seismic examples from the southern North Sea. *In*: Cooper, M.A. & Williams G.D. (eds) *Inversion Tectonics*, Geological Society, London, Special Publications, **44**, 201-219.

Bray, R.J., Green P.F. & Duddy I.R. 1992 Thermal history reconstruction using apatite fission track analysis and vitrinite reflectance: a case study from the U.K. East Midlands and southern North Sea. *In*: Hardman R.F.P. (ed) *Exploration Britain: geological insights for the next decade* Geological Society, London, Special Publications, **67**, 3-25.

Burnham, A.K. & Sweeney, J.J. 1989. A chemical kinetic model of vitrinite reflectance maturation. *Geochimica et Cosmochimica Acta*, **53**, 2649-2657.

David, M.J. 1996. History of hydrocarbon exploration in the Moray Firth. *In*: Hurst A., Johnson, H.D., Burley, S.D., Canham, A.C. & Mackertich, D.S. (eds) *Geology of the Humber Group: Central Graben and Moray Firth, UKCS.* Geological Society, London, Special Publications, **114**, 47-80.

Duncan, W.I., Green, P.F. & Duddy, I.R. 1998. Source Rock Burial History and Seal Effectiveness: Key Facets to Understanding Hydrocarbon Exploration Potential in the East and Central Irish Sea Basins. *American Association of Petroleum Geologists Bulletin*, **82,** 1401-1415.

Galbraith, R.F. & Laslett, G.M. 1993. Statistical methods for mixed fission track ages. *Nuclear Tracks*, **21**, 459-470.

Gibson, J.R., Walsh, J.J. & Watterson, J. 1989. Modelling of bed contours and cross-sections adjacent to planar normal faults. *Journal of Structural Geology*, **11**, 317-328.

Glennie, K.W. & Underhill, J.R. 1998. The Development and Evolution of Structural Styles in the North Sea. *In*: Glennie, K. (ed.) *Introduction to the Petroleum Geology of the North Sea (4th edition)*, Blackwell Science, 42-84.

Green P.F. 1986. On the thermo-tectonic evolution of Northern England: evidence from fission track analysis. *Geological Magazine*, **123**, 493 - 506.

Green, P.F., Duddy I.R., Gleadow A.J.W. & Lovering J.F. 1989a. Apatite fission track analysis as a palaeotemperature indicator for hydrocarbon exploration. *In*: Naeser N.D. & McCulloh, T. (eds) *Thermal history of sedimentary basins-methods and case histories*. Springer-Verlag, New York, 181-195.

Green, P.F., Duddy, I.R., Laslett, G.M., Hegarty, K.A., Gleadow, A.J.W. & Lovering, J.F. 1989b. Thermal annealing of fission tracks in apatite 4. Quantitative modelling techniques and extension to geological timescales: *Chemical Geology (Isotope Geoscience Section)*, **79**, 155-182.

Green, P.F., Duddy, I.R. & Bray, J.R. 1995. Applications of thermal history reconstruction in inverted basins. *In*: Buchanan, J.G. & Buchanan, P.G. (eds) *Basin Inversion*: Geological Society, London, Special Publications, **88**, 149-165.

Green, P.F., Hegarty, K.A. & Duddy, I.R. 1996. Compositional influences on fission track annealing in apatite and improvement in routine application of AFTA®. American Association of Petroleum Geologists, San Diego, Abstracts with Program, A.56.

Green, P.F., Thomson, K. & Hudson, J.D. 2001a. Recognising tectonic events in undeformed regions: contrasting results from the Midland Platform and East Midlands Shelf, Central England. *Journal of the Geological Society, London*, **158**, 59-73.

Green, P.F., Duddy, I.R., Bray, R.J, Duncan, W.I. & Corcoran, D. 2001b. Thermal history reconstruction in the Central Irish Sea Basin. *In*: Shannon, P.M., Haughton, P.M. & Corcoran, D. (eds.) *Petroleum Exploration of Ireland's Offshore Basins* Geological Society, London, Special Publications, **188**, 171-188.

Green, P.F., Duddy, I.R. & Hegarty, K.A. in press, Quantifying exhumation in sedimentary basins of the UK from apatite fission track analysis and vitrinite reflectance data: precision, accuracy and latest results. *In:* Dore, A.G., Cartwright, J.A., Stoker, M.S., Turner, J.P. & White, N.J. (eds.). *Exhumation of the Circum-Atlantic Margins* Geological Society, London, Special Publication.

Hallam, A. 1963. Major epeirogenic and eustatic changes since the Cretaceous, and their possible relationships to crustal structure. *American Journal of Science*, **261**, 397-423.

Harland, W.B., Armstrong, R.L., Cox, A.V., Craig, L.E., Smith, A.G. & Smith, D.G. 1989. *A geologic time scale 1989*, Cambridge University Press.

Hillis, R.R., Thomson, K. & Underhill, J.R. 1994. Quantification of Tertiary erosion in the Inner Moray Firth using sonic velocity data from the Chalk and the Kimmeridge Clay. *Marine and Petroleum Geology*, **11**, 283-293.

Hurford, A.J.H. & Green, P.F. 1983. The zeta age calibration of fission-track dating: *Chemical Geology (Isotope Geoscience Section)*, **1**, 285-317.

Hutton, A.C., Kantsler, A.J., Cook, A.C. & McKirdy, D.M. 1980. Organic matter in oil shales. *Journal of the Australian Petroleum Exploration Association*, **20**, 44-67.

Jackson, J.A., White, N.J., Garfunkel, Z. & Anderson, H. 1988. Relations between normal-fault geometry, tilting and vertical motions in extensional terrains: an example from the southern Gulf of Suez. *Journal of Structural Geology*, **10**, 155-170.

Japsen, P. 1997. Regional Neogene exhumation of Britain and the western North Sea. *Journal of the Geological Society, London*, **154**, 239-247.

Japsen, P. 1999. Overpressured Cenozoic shale mapped from velocity anomalies relative to a baseline for marine shale, North Sea. *Petroleum Geoscience*, **5**, 321-336.

McKenzie, D. 1984. A possible mechanism for epeirogenic uplift. *Nature*, **307**, 616-618.

McQuillin, R., Donato, J.A. & Tulstrup, J. 1982. Development of basins in the Inner Moray Firth and the North Sea by crustal extension and dextral displacement of the Great Glen Fault. *Earth Planetary Scientific Letters*, **60**, 127-139.

Pazzaglia, F.J. & Gardner, T.W. 1994. Late Cenozoic flexural deformation of the middle United-States Atlantic passive margin. *Journal of Geophysical Research – Solid Earth,* **99**, 12143-12157.

Price, L.C. & Barker, C.E. 1985. Suppression of vitrinite reflectance in amorphous rich kerogen-a major unrecognized problem. *Journal of Petroleum Geology*, **8**, 59-84.

Rattey, R.P. & Hayward, A.B. 1993. Sequence stratigraphy of a failed rift system: the Middle Jurassic to Early Cretaceous basin evolution of the Central and Northern North Sea. *In*: Parker, J.R. (ed) *Petroleum geology of Northwest Europe: Proceedings of the 4th Conference,* The Geological Society, London, 215-249.

Roberts, A.M. & Holdsworth, R.E. 1999. Linking onshore and offshore structures: Mesozoic extension in the Scottish Highlands. *Journal of the Geological Society, London*, **156**, 1061-1064.

Rohrman, M. & van der Beek, P. 1996. Cenozoic postrift domal uplift of North Atlantic margins: An asthenospheric diapirism model. *Geology*, **24**, 901-904.

Russell, L.R. & Busby-Spera, C.J. 1992. Structural style and tectonic evolution of the Rio Grande Rift, New Mexico, U.S.A. *In*: Landon, S.M. (ed) *Interior rift basins*. American Association of Petroleum Geologists Memoir, **59**, 205-258.

Stewart, S.A. 1996. Tertiary extensional fault systems on the western margin of the North Sea Basin. *Petroleum Geoscience*, **2**, 167-176.

Thomson, K. & Underhill, J.R. 1993. Controls on the development and evolution of structural styles in the Inner Moray Firth. *In*: Parker, J.R. (ed) *Petroleum geology of Northwest Europe: Proceedings of the 4th Conference,* The Geological Society, London, 1167-1178

Thomson, K., Underhill J.R., Green, P.F., Bray, R.J. & Gibson, H.J. 1999. Evidence from apatite fission track analysis for post-Devonian burial and exhumation history of the northern Highlands, Scotland. *Marine and Petroleum Geology,* **16**, 27-39.

Underhill, J.R. 1991a. Implications of Mesozoic-Recent basin development in the Inner Moray Firth, UK. *Marine and Petroleum Geology*, **8**, 359-369.

Underhill, J.R. 1991b. Controls on Late Jurassic seismic sequences, Inner Moray Firth, UK North Sea: a critical test of a key segment of Exxon's original sea-level chart. Basin Research, 3, 79-98.

Underhill, J.R. 1998. Jurassic. *In*: Glennie, K. (ed.) *Introduction to the Petroleum Geology of the North Sea (4th Edition)*, Blackwell Science, 245-293.

Underhill, J.R. & Partington, M.A. 1993. Jurassic thermal doming and deflation in the North Sea: Implications of sequence stratigraphic evidence. *In*: Parker, J.R. (ed) *Petroleum geology of Northwest Europe: Proceedings of the 4th Conference,* The Geological Society, London, 337-345.

Figure Captions

Figure 1a

Location map of study area in the context of the North Sea rift system (Moray Firth location shown on inset map). Main map shows database of 2D seismic data and wells superimposed on map of geology at sea bed, modified in this study after Andrews et al., (1990). Note that Tertiary and Chalk are absent in the Inner Moray Firth, note also the extensional faulted displacements of the base Upper Cretaceous and Base Tertiary, key evidence for significant post Cretaceous faulting in the basin. Key wells discussed in this paper are labelled.

Figure 1b

Generalized stratigraphy of the Moray Firth including erosion due to Tertiary regional uplift in the Inner Moray Firth.

Figure 2

Top Triassic surface within the Inner Moray Firth illustrating the well-developed post-Triassic rift architecture of the basin. Location of the seismic line shown in Figure 3 is marked.

Figure 3

Seismic section illustrating the reactivation of earlier Jurassic structures with faults subcropping the sea bed. Vertical scale is in seconds TWT (Two way travel time). Vertical exaggeration of this regional line is approximately x15. The largest faults in the Inner Moray Firth have up to 2km offset of the Base Jurassic sequences. Many faults offset the Base Cretaceous with throws in the range 10 - 300 metres. So although these structures are principally Mesozoic in age, they have a significant post-Jurassic history of reactivation, in contrast with the deeper North Sea sub-basins. Purple pick is Top Jurassic, Blue pick is Base Jurassic.

Figure 4

VR data from Inner Moray Firth exploration wells against depth shows a wide variance of values, although individual wells exhibit consistent reflectance gradients. Notwithstanding the scatter in the dataset as a whole, the VR recorded by the majority of the wells is found to be higher than that expected for its equivalent sample depth when compared to their counterparts in the Outer Moray Firth. As indicated here, this can be interpreted as exhumation.

Figure 5

Sonic log data for the Inner Moray Firth, from Hillis et al (1994). Inset graph illustrates the relationship between mean sonic slowness and depth to the unit midpoint plot for the Kimmeridge Clay Formation. The linear normal or undisturbed, compaction relationship is also shown. From this data Hillis et al (1994) produced a total erosion map for the Inner Moray Firth reflecting the variation in exhumation across the basin (main map).

Figure 6

If the palaeogeothermal gradient can be constrained by AFTA and VR, then for an assumed value of surface temperature, Ts, the amount of section removed can be estimated, as shown. See Bray et al (1992) for more details.

Figure 7

AFTA parameters plotted against sample depth and present temperature for samples from wells 12/23-1 and 12/24-2. The variation of stratigraphic age with depth in each well is also shown, as the solid line in the central panel. See text for detailed discussion.

Figure 8

Measured fission track ages in individual apatite grains from sample GC237-30 (well 12/23-10 and sample GC237-55 (well 12/24-2), plotted against Cl content (measured by electron microprobe). Results from each sample are compared with the pattern predicted from the respective "Default Thermal History", i.e. the pattern exppected if the sample had not been hotter than its present temperature at any time since deposition. Measured ages in the sample from well 12/23-1 are much less than the predicted values, whereas results from well 12/24-2 are generally older than predicted. This shows that while the sample from well 12/23-1 has been hotter in the past, the sample from 12/24-2 is now at (or close to) its maximum post-depositional palaeotemperature.

Figure 9

Comparison of the timing information derived from AFTA data in all samples in this study showing evidence for higher palaeotemperatures at some time after deposition. Comparison of timing in all samples suggests that cooling began between 55-60 Ma, as shown by the vertical green region. Grey box in each row indicates the range of depositional ages for individual samples. Black box in each row defines the range of timing for the onset of cooling derived from AFTA data in each sample within a 95% confidence interval. Vertical grey box crossing all samples shows zone of overlap of all AFTA data.

Figure 10

a) Palaeotemperature constraints derived from AFTA and VR in well 12/23-1, plotted against TVD(RKB). Open circles refer to corrected BHT values. Red circles show palaeotemperatures from VR. Horizontal bars and arrows denote palaeotemperature constraints from AFTA. The burial and exhumation history reconstruction derived from this data involves deeper burial on the post-Cretaceous unconformity in this well, with an additional 1150m of section removed by Tertiary exhumation and erosion. The Default burial history derived from the preserved section, together with a sea-bed temperature of 6C and a present-day geothermal gradient of 29.7C/km is also shown.

b) Palaeotemperature constraints derived from AFTA and VR in well 12/24-2, plotted against TVD(RKB). Symbols are as above. The burial and exhumation history reconstruction derived from this data show no evidence of any palaeothermal events. Therefore this reconstruction is identical to the Default burial history derived from the preserved section, together with a sea-bed temperature of 6C and a present-day geothermal gradient of 32.4C/km.

Figure 11

A seismic line tying wells 12/23-1 and 12/24-2 clearly shows a post-Jurassic history of extensional movement on the Smith Bank Fault. Annotation as in Figure 3. Vertical exaggeration of this line is approximately x9. The depths to Base Jurassic and Cretaceous in the wells, tied to the seismic image with well control indicate that there has been 2,350m of post Triassic displacement on the Smith Bank Fault, of which 750m is post-Jurassic. The AFTA and VR estimates of differential exhumation between these two wells in this study, and those of Hillis et al 1994, are consistent with the seismically-observed post-Jurassic offset of 750±30m.

Figure 12

We define three end member kinematic models that could account for exhumation of the Inner Moray Firth, these models being characterised by various combinations of regional exhumation (on a wavelength of 100's km) and fault – controlled differential local exhumation.

a) Notional rift basin template. Note position of datums.

b) We term the case where there is little or no contribution from intra-basinal faulting during regional exhumation as 'homogenous' exhumation. Such exhumation would lead to smooth, progressive variations in exhumation. At the other extreme, exhumation could result from some contribution of reverse faulting. This defines a second kinematic possibility:

c) Basin wide inversion controlled by numerous reverse faults, that give a heterogeneous picture of basin inversion, combined with some contribution of regional exhumation (the same amount as shown in part b).

d) A third kinematic model combines a background of regional, homogeneous exhumation accompanied by extensional faulting. If the entire plate that is being extensionally faulted is also regionally exhumed, the absolute amount hangingwall and footwall exhumation will be different. Both sides of the extensional fault may become exhumed relative to regional datums, in spite of the extension across the fault. Downthrow of the hangingwall is essentially buffered by the regional exhumation. Note that the stratigraphy and burial history encountered in the highlighted hangingwall well is essentially the same as that in the non-inverted scenario shown in (a).

Table 1: Sample details and apatite fission track age data for samples from two Inner Moray Firth wells

Sample number GC237-	Depth (m)	Stratigraphic details*1	ρ_D*2 (10^6 tracks /cm^2)	ρ_s*2 (10^6 tracks /cm^2)	ρ_i*2 (10^6 tracks /cm^2)	Zeta	Pooled / Central fission track age*3 (Ma)	P(χ^2) (%) (no. of grains)	Mean track length*4 (μm)
12/23-1									
27	869-905	M. – L. Oxfordian (157-156 Ma)	1.340 (2105)	2.074 (1181)	1.500 (854)	360.3 ± 6.8	330.8 ± 29.3	<1 (20)	11.77 ± 0.20 (101)
28	1225-1356	U. Permian - Triassic (256-208 Ma)	1.339 (2105)	3.316 (1847)	2.613 (1455)	360.3 ± 6.8	301.9 ± 17.4	<1 (20)	11.17 ± 0.17 (103)
29	1676-1813	L. Permian (290-256 Ma)	1.337 (2105	2.685 (1784)	2.149 (1428)	360.3 ± 6.8	268.1 ± 22.6	<1 (20)	10.76 ± 0.20 (121)
30	2565-2566	Devonian (408-363 Ma)	1.336 (2105	1.059 (753)	3.454 (2456)	360.3 ± 6.8	76.1 ± 10.8	<1 (20)	10.42 ± 0.24 (105)
12/24-2									
55	2676-2685	L. Volgian (152-150 Ma)	1.668 (2608)	1.144 (742)	2.757 (1789)	360.3 ± 6.8	117.2 ± 21.9	<1 (20)	8.84 ± 0.25 (110)
56	3596-3673	Triassic (208-245 Ma)	1.663 (2608)	0.563 (430)	2.074 (1583)	360.3 ± 6.8	30.6 ± 10.7	<1 (20)	9.67 ± 0.53 (27)

*1 All numerical values for stratigraphic ages assigned following Harland (1989).
*2 Numbers in parentheses show the number of tracks counted in determining all track densities.
*3 Central age (Galbraith and Laslett, 1993), used for samples containing a significant spread in single grain ages ($P(\chi^2)<5\%$).
*4 Numbers in parentheses show the number of track lengths measured.

All analytical details are as described by Green (1986), with the exception that some thermal neutron irradiations show a significant flux gradient, in which case the appropriate value of ρ_D was determined by linear interpolation through the stack of grain mounts.

Table 2: Thermal history interpretation summary of AFTA and VR data in two Inner Moray Firth wells

Sample number GC237-	Depth (m)	Stratigraphic details[*1]	Present temperature (°C)	Default VR / AFTA parameters[*2]	Measured VR[*3] (%)	Maximum paleo-temperature[*4] (°C)	Onset of cooling from AFTA (Ma)
12/23-1							
	236	M. Barremian (130-128 Ma)	11	0.27	0.30	<50	
	312	L. Barremian (131-130 Ma)	13	0.27	0.29	<50	
	543	L. Barremian-Hauterivian (133-131 Ma)	19	0.28	0.28	<50	
	776	L. Valanginian (141-138 Ma)	26	0.28	0.33	50	
	792	U. – M. Volgian (150-146 Ma)	27	0.28	0.28	<50	
	808	M. Volgian (152-150 Ma)	27	0.29	0.31	<50	
	823	M. Volgian (152-150 Ma)	28	0.29	0.30	<50	
	853	U.-M. Oxfordian (156-155 Ma)	29	0.30	0.32	50	
27	869-905	M.-L. Oxfordian (157-156 Ma)	30	150 Ma 14.2 µm		65-85	100-15
28	1225-1356	U. Permian - Triassic (256-208 Ma)	42	221 Ma 13.6 µm		75-95	100-15
29	1676-1813	L. Permian (290-256 Ma)	55	231 Ma 12.9 µm		80-105	190-10
	1897	L. Permian (290-256 Ma)	60	0.45	0.55	92	
30	2565-2566	Devonian (408-363 Ma)	80	229 Ma 9.9 µm		>100	120-40
12/24-2							
55	2676-2685	L. Volgian (152-150 Ma)	90	37 Ma 10.1 µm		<110	post-deposition
	2681	L. Volgian (152-150 Ma)	90	0.63	0.50 (30)	69	
	2856	Kimmeridgian (155-152 Ma)	96	0.66	0.55 (27)	78	
	3136	U. –M. Oxfordian (156-155 Ma)	105	0.73	0.67 (15)	95	
56	3596-3673	Triassic (208-245 Ma)	121	2 Ma 8.9 µm		<125	post-deposition

[*1] All numerical values for stratigraphic ages assigned following Harland (1989).
[*2] Values of vitrinite reflectance (for VR samples) or fission track age and mean track length (for AFTA samples) predicted from the respective "Default Thermal History" (as defined in the text) for each sample.
[*3] Numbers in parentheses show the number of fields measured, where available.
[*4] Thermal history interpretation has been carried out using methods outlined by Green et al. (2001).

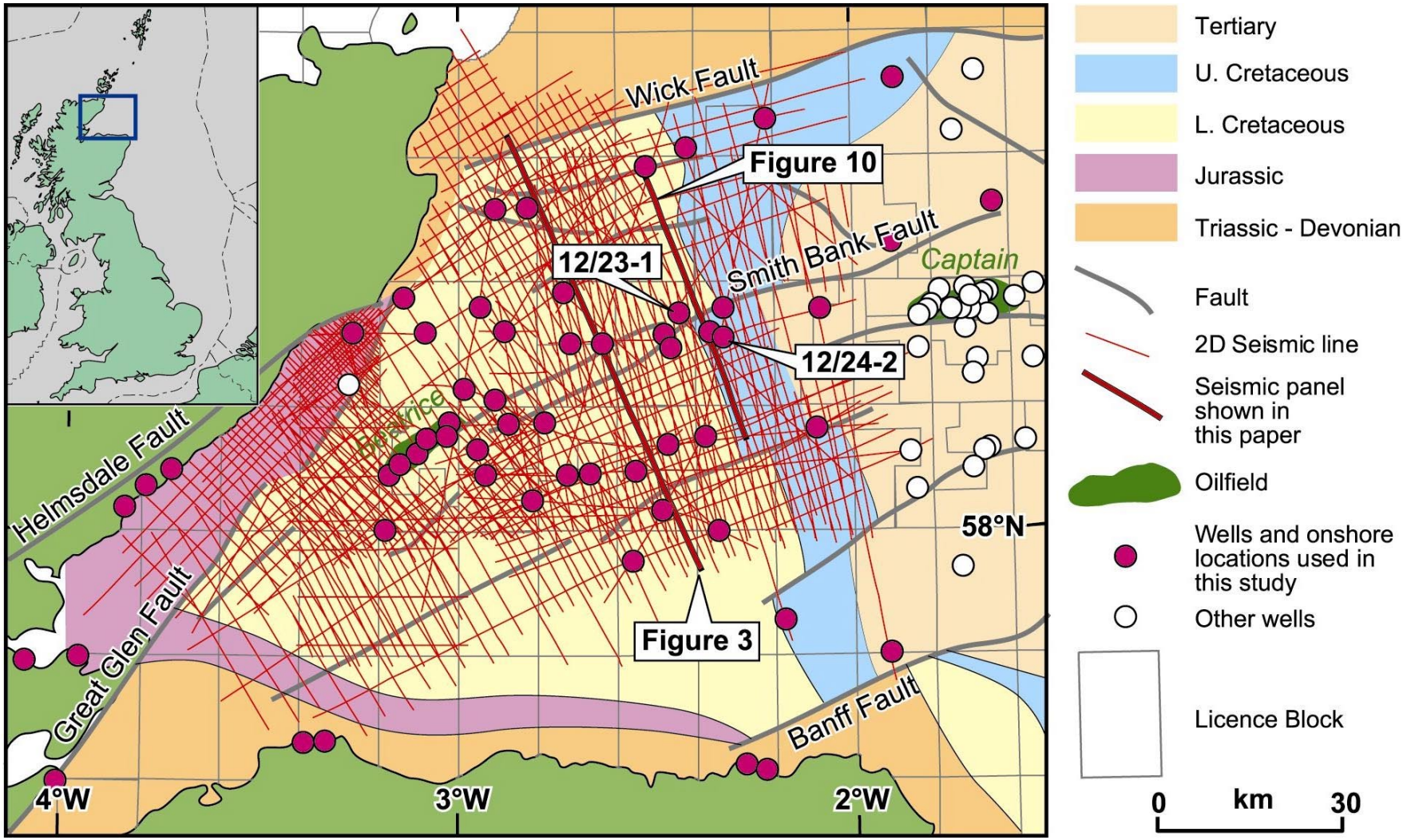

Argent et al Figure 1a

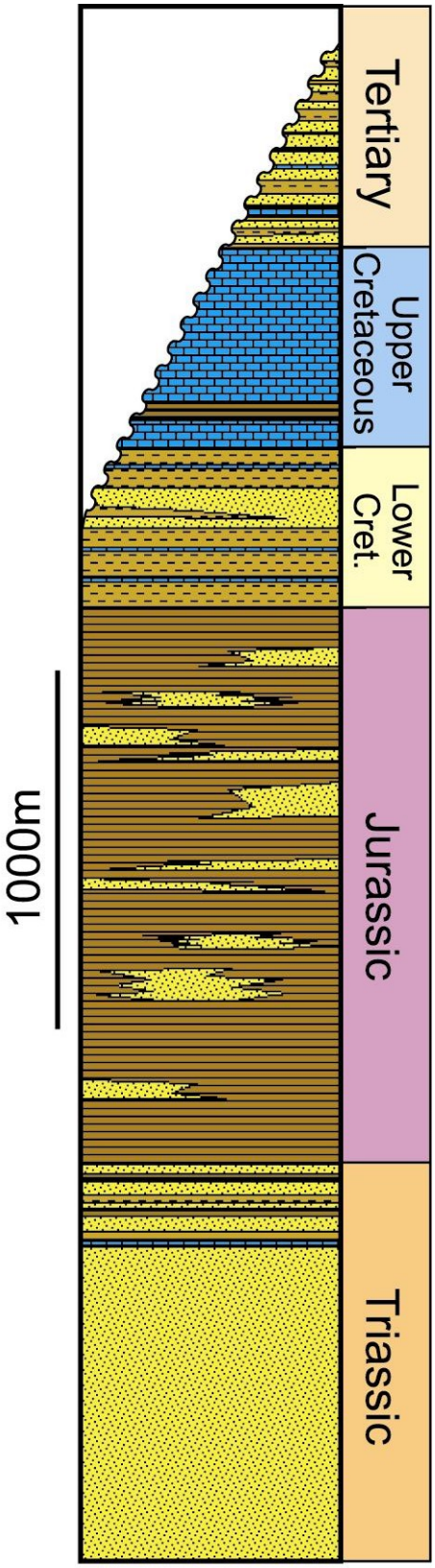

Argent et al Figure 1b

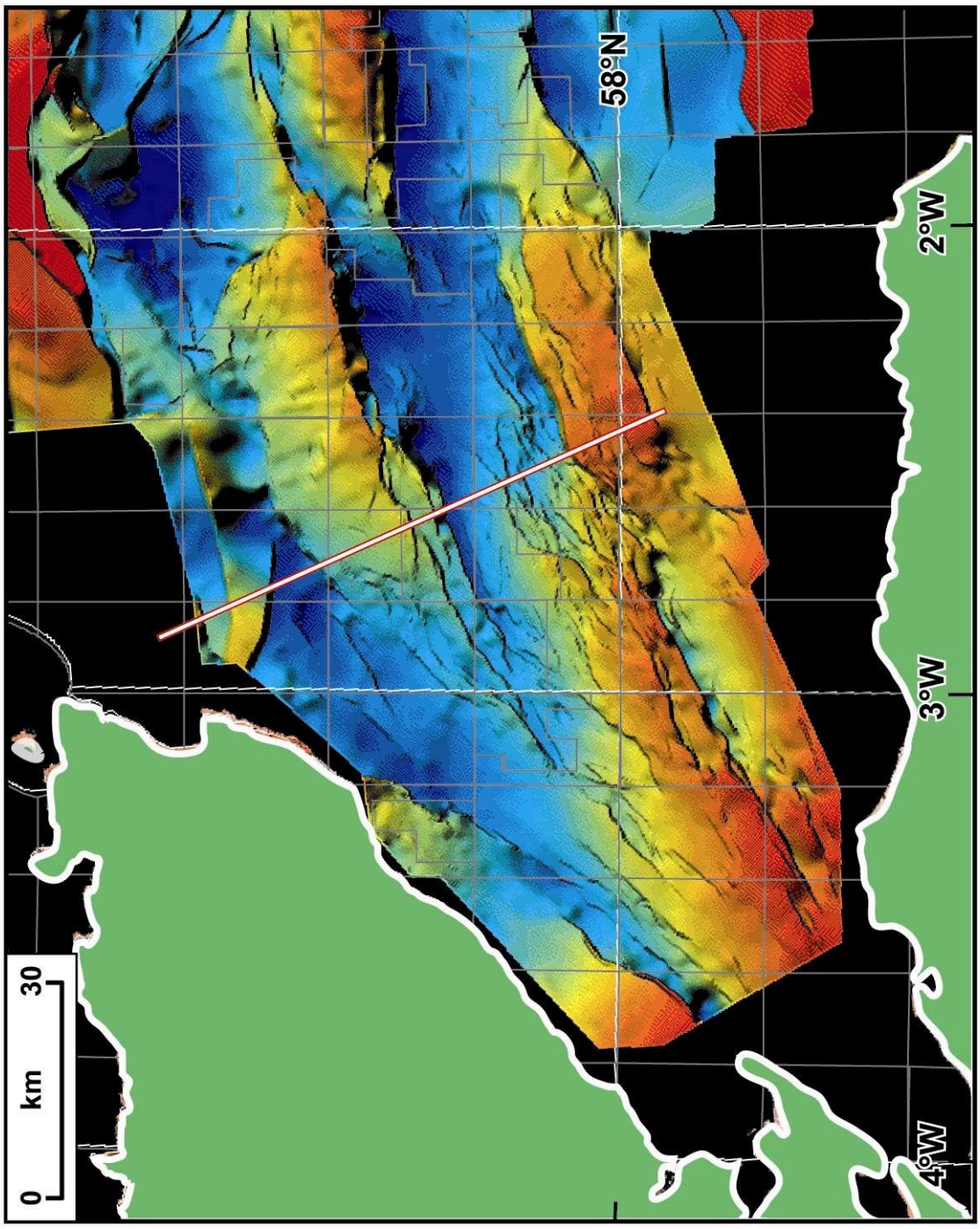

Argent et al Figure 2

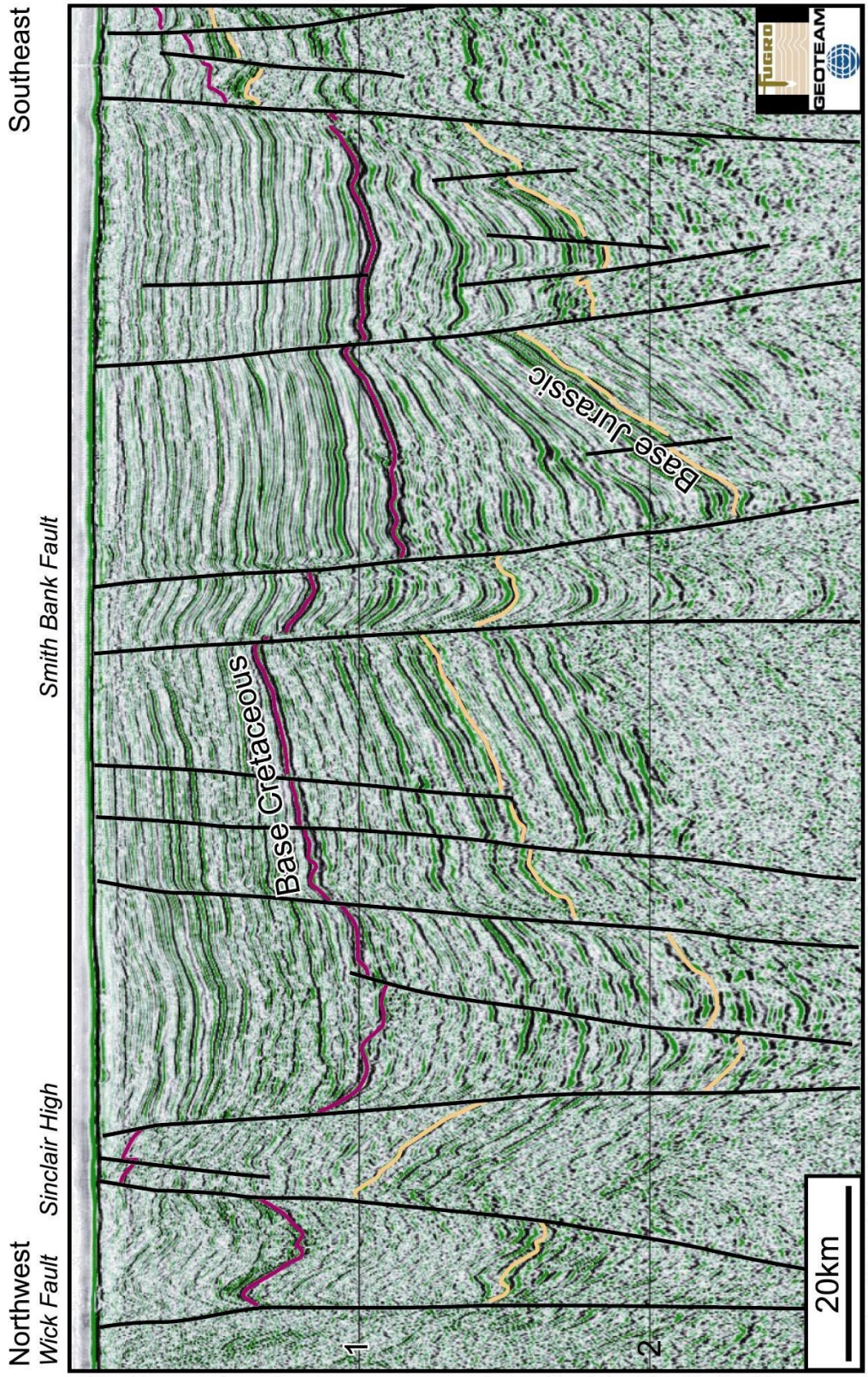

Argent et al Figure 3

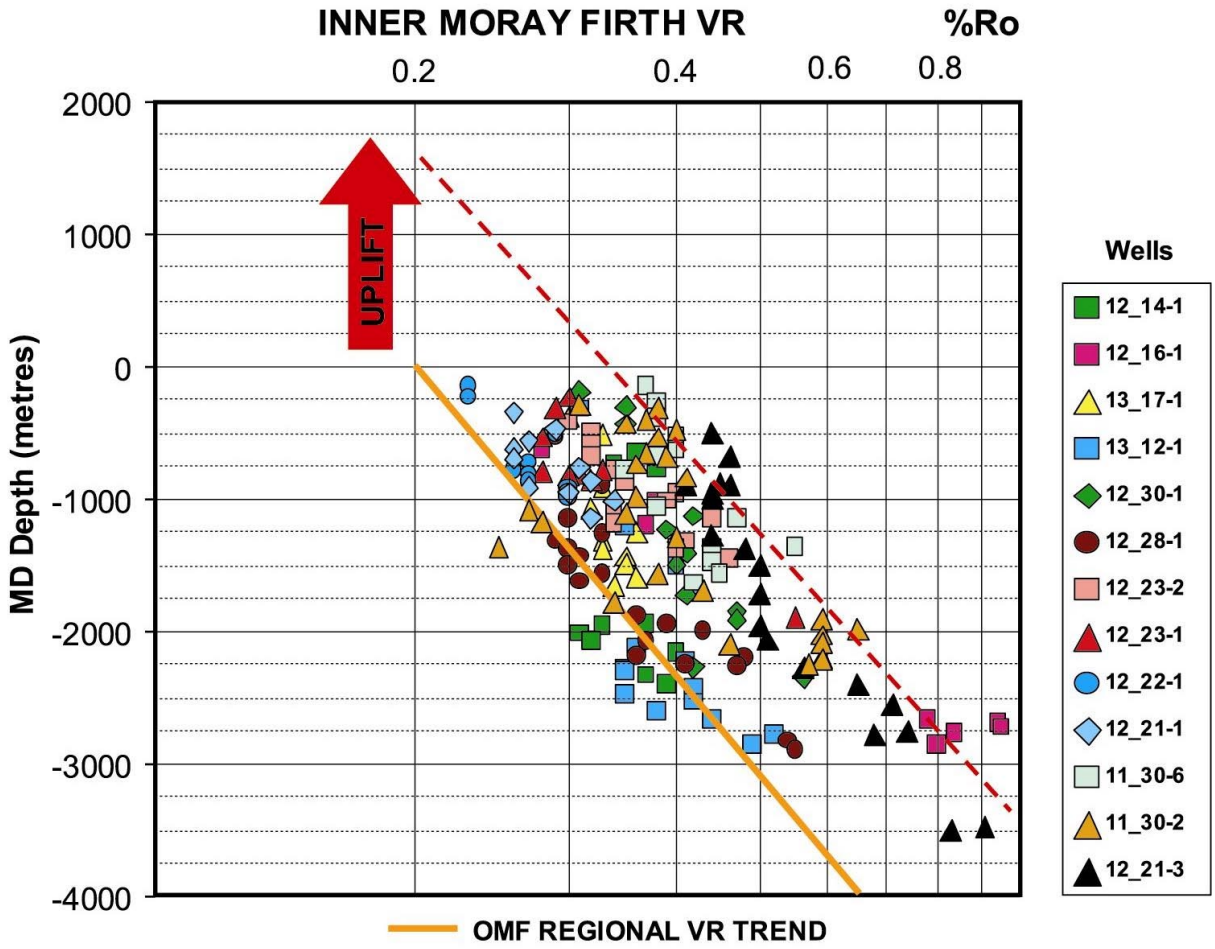

Argent et al Figure 4

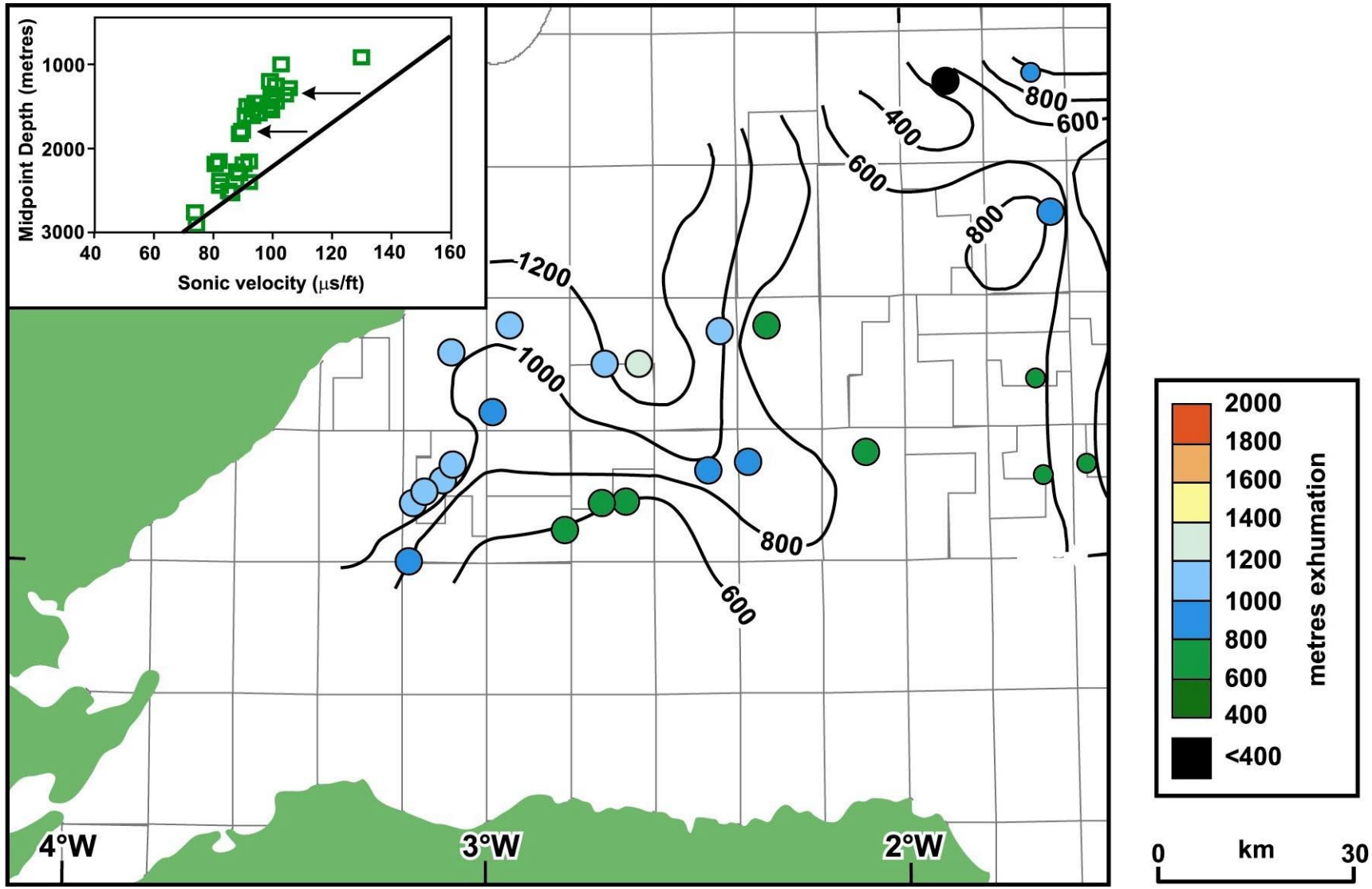

Argent et al Figure 5

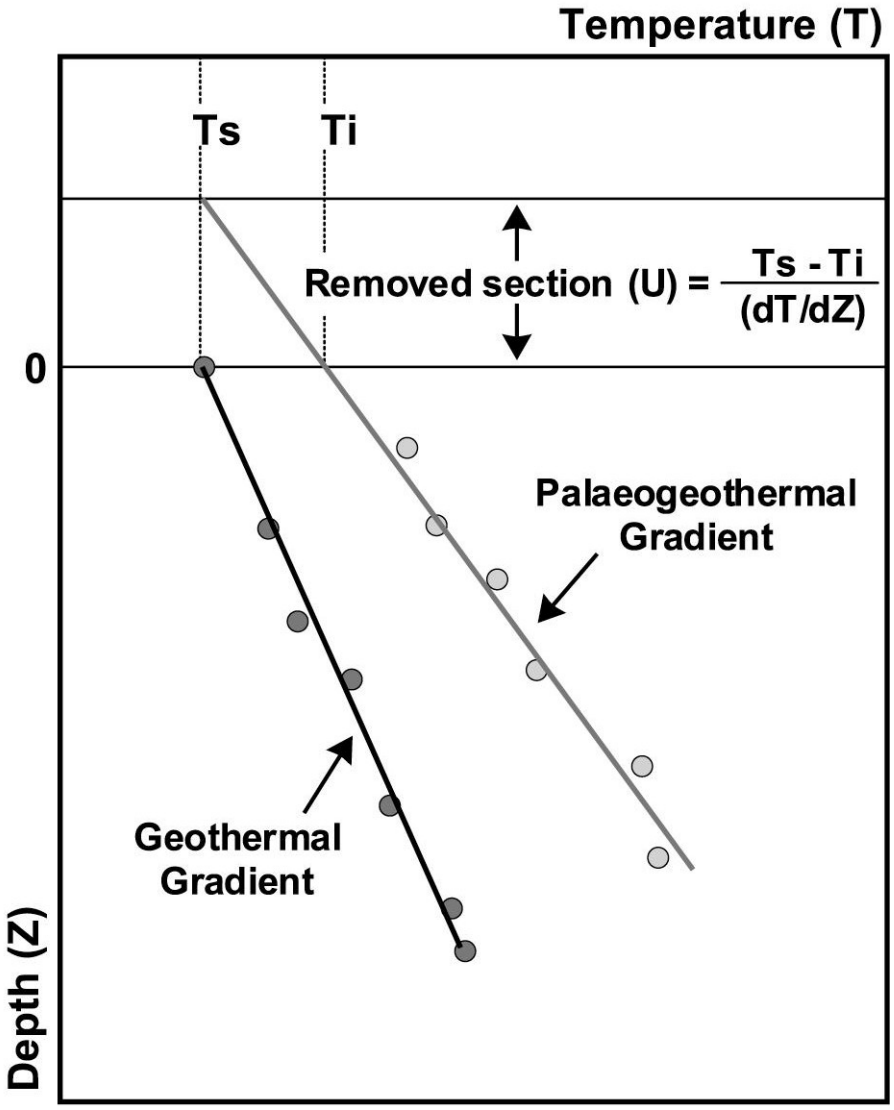

Argent et al Figure 6

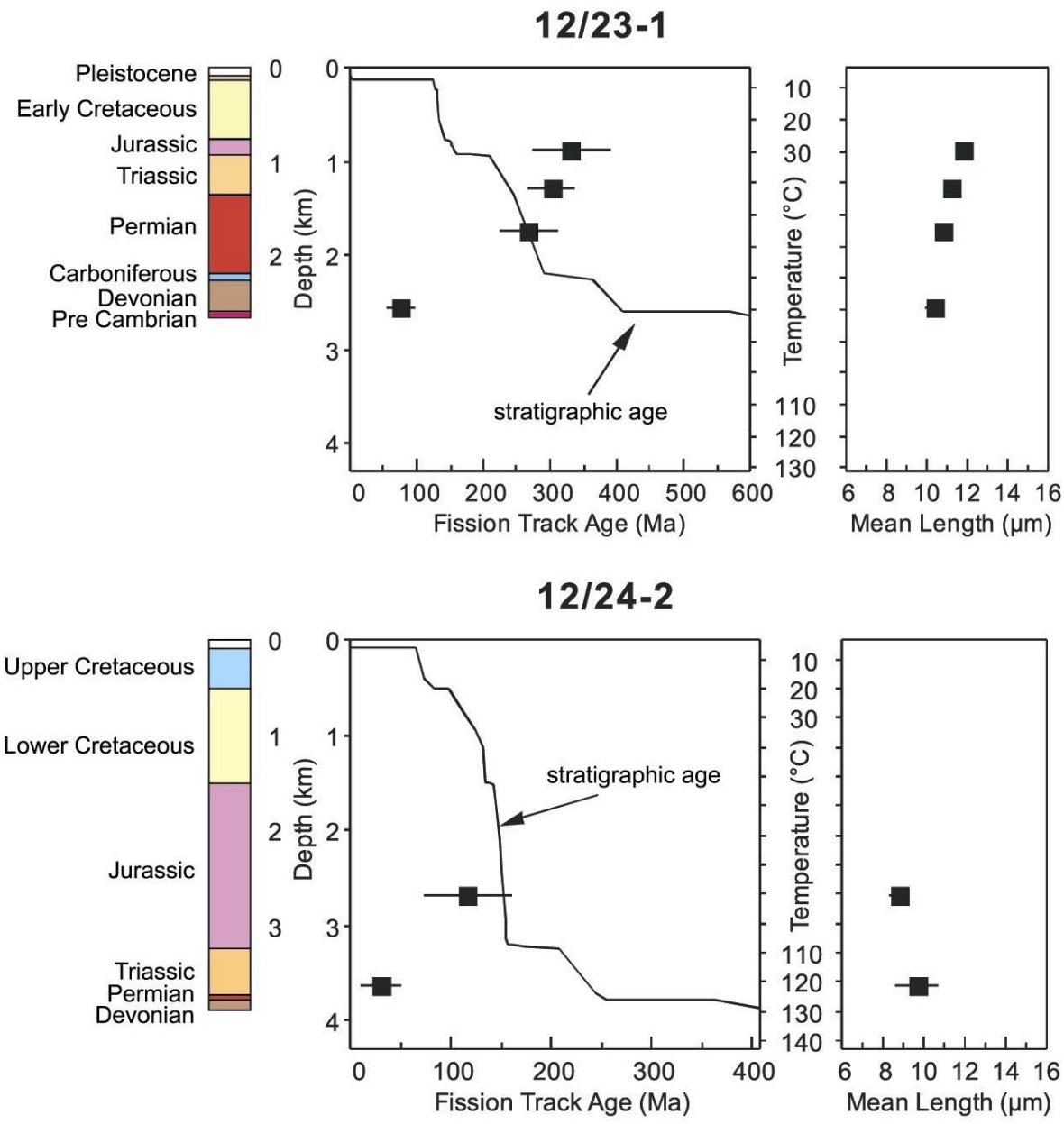

Argent et al Figure 7

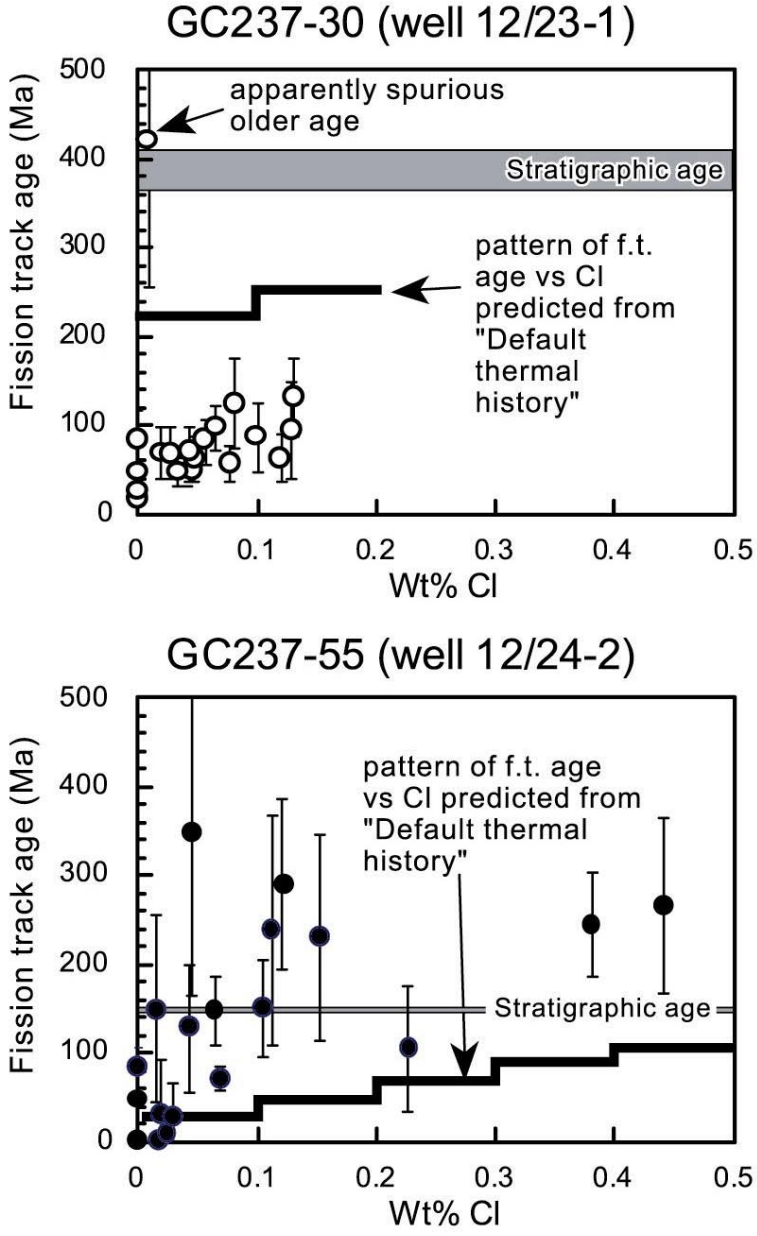

Argent et al Figure 8

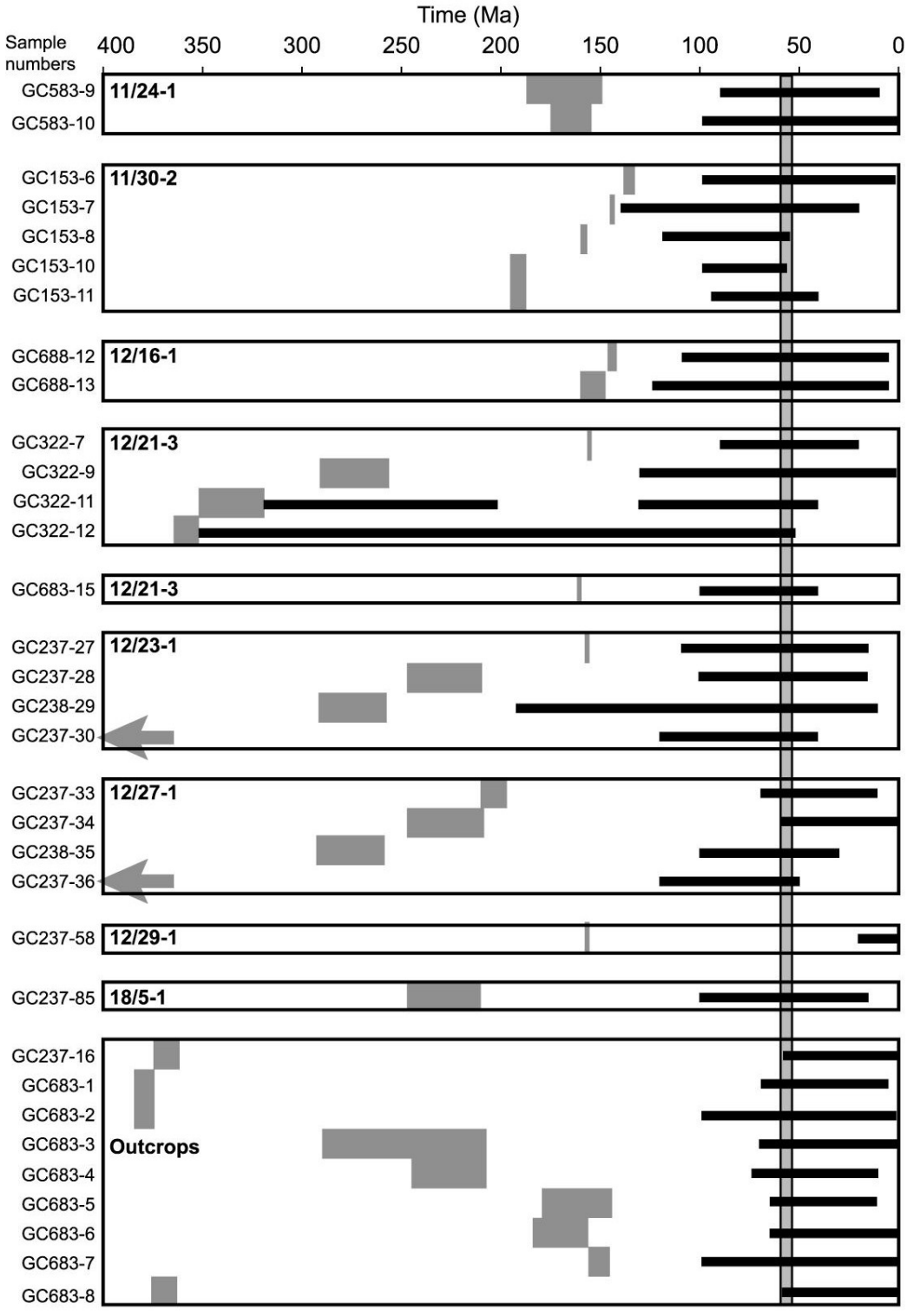

Argent et al Figure 9

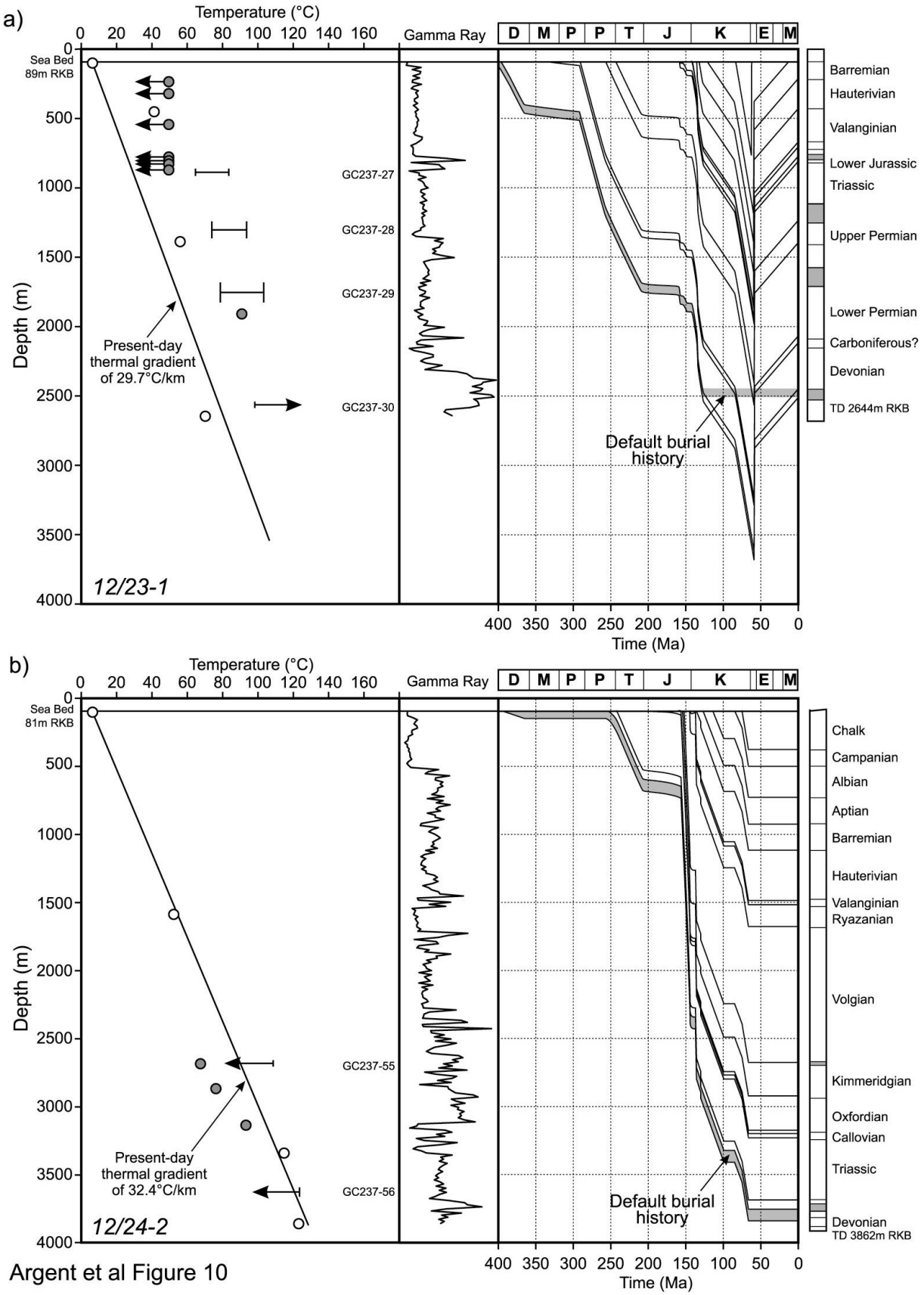

Argent et al Figure 10

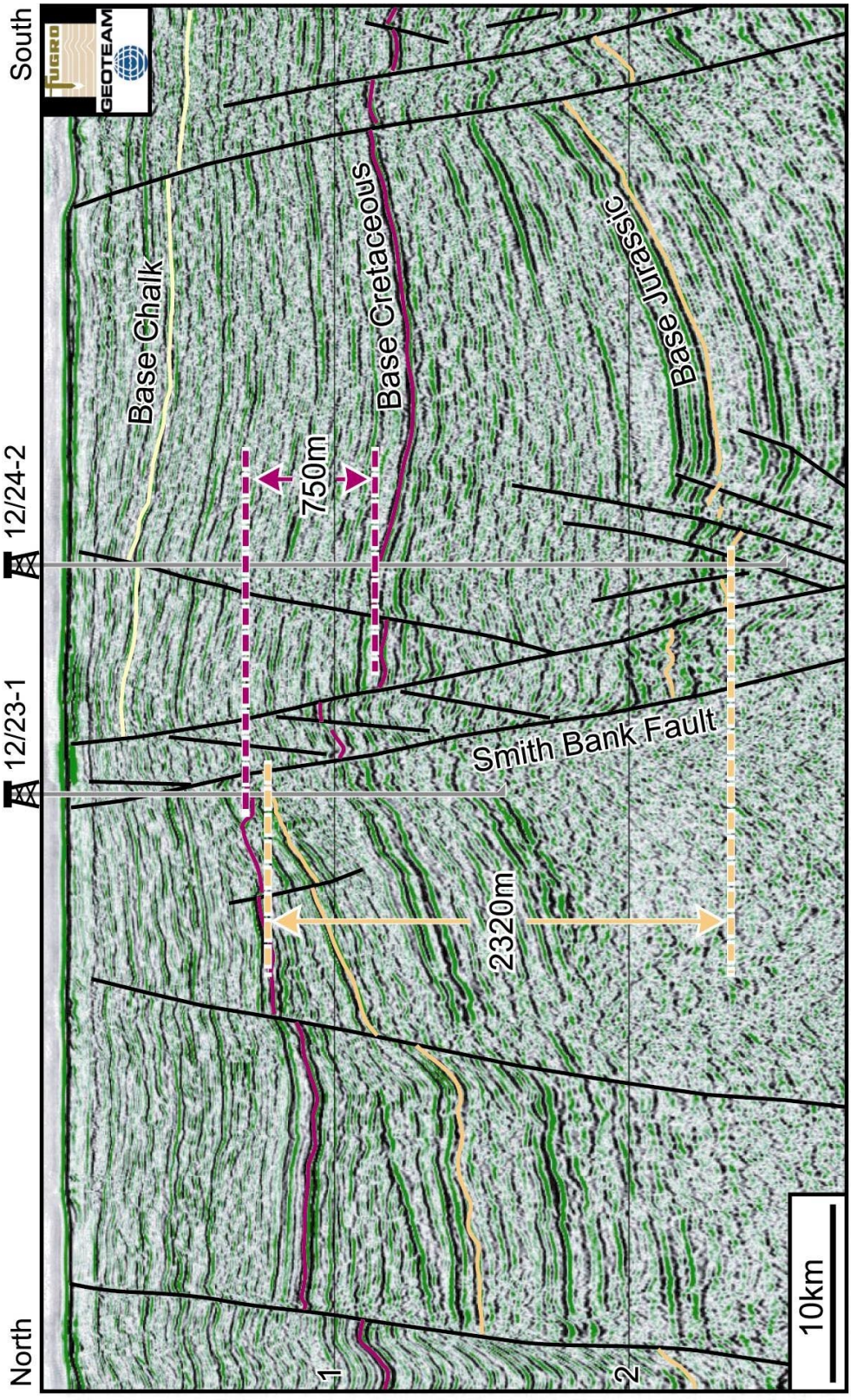

Argent et al Figure 11

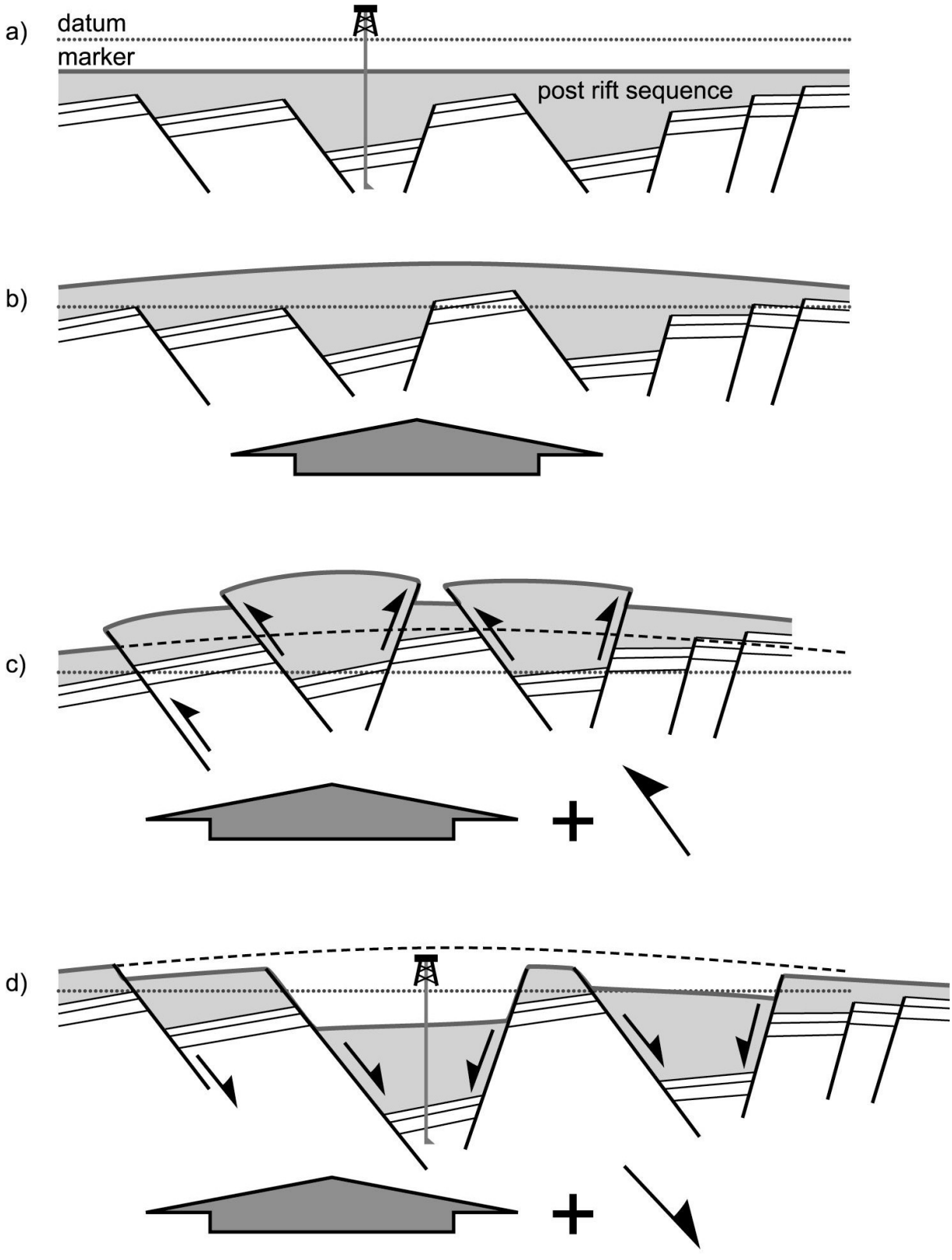

Argent et al Figure 12